

Experimental evidence of covalent bond character of the central O-H-O fragment in the Zundel cation

Supplement

Krešimir Molčanov^a, Christian Jelsch^b, Emmanuel Wenger^b, Jernej Stare^c, Anders Ø. Madsen^d,
Biserka Kojić-Prodić^a

^aRudjer Bošković Institute, Bijenička 54, HR-10000 Zagreb, Croatia

^bCristallographie, Résonance Magnétique et Modélisations CNRS, UMR 7036, Institut Jean Barriol,
CNRS and Université de Lorraine BP 70239, F54506 Vandoeuvre-lès-Nancy CEDEX, France

^cNational Institute of Chemistry, Hajdrihova 19, SI-1000 Ljubljana, Slovenia

^dDepartment of Pharmacy, University of Copenhagen, Universitetsparken 2, 2100 København,
Denmark

e-mail: kmolcano@irb.hr, christian.jelsch@univ-lorraine.fr

S1 Experimental details and residual density

S2 Periodic DFT calculations

S3 Charge density of the nitranilate dianion

S4 Hirshfeld surface and contacts

S5 References

S1 Experimental details and residual density

The single crystals of nitranilic acid hexahydrate were prepared as described previously.¹ A lustrous orange prismatic-like specimen of $C_4H_3N_2O_5$, approximate dimensions 0.050 mm x 0.060 mm x 0.160 mm, was used for the X-ray crystallographic analysis. X-ray diffraction measurements were performed on a Bruker D8 Venture diffractometer at 100(2) K using $MoK\alpha$ radiation, to the maximum resolution of 0.50 Å. A total of 6399 frames were collected and the total exposure time was 53.33 hours. The frames were integrated with the Bruker SAINT² software package using a narrow-frame algorithm. The integration of the data using a monoclinic unit cell yielded a total of 66 115 reflections to a maximum θ angle of 45.50° (0.50 Å resolution), of which 5323 were independent (average redundancy 12.4, completeness = 99.5 %, $R_{int} = 7.27$ %, $R_{sig} = 3.67\%$) and 3576 were greater than $3\sigma(F^2)$. Data were corrected for absorption effects using the multi-scan method (SADABS).³ The multiple integrated reflections were averaged for the space group $P 2_1/c$ using SORTAV⁴ adapted to area detector data. Spherical-atom model was refined using SHELXL-97;⁵ atomic coordinates were taken from the room-temperature structure.¹ Multipolar refinement was carried out with program package MoPro⁶ vs. all reflections F^2*2 up to $s = 0.9 \text{ \AA}^{-1}$, reflections beyond this resolution were omitted due to Y_{obs}/Y_{calc} improper scaling (Fig. S6). To correct for thermal diffuse scattering,⁷ a polynomial scale factor (monotonous increasing function of $s=\sin\theta/\lambda$) was refined and applied ($K = 0.06083 + 0.00771 s^4$).

The lengths of the O-H bonds in water and Zundel molecules were restrained to 0.983(2) Å, and hydrogen atoms were refined as anisotropic, with their U_{iso} s constrained to values derived from quantum chemical calculations: the vibrational modes were calculated by *Crystal14*^{8,9} and the U_{iso} s were then estimated by the SHADE3 server.¹⁰

The Zundel proton H1, which is bound to two oxygen atoms, was refined with no distance restraints. Its electron density was modelled as one dipole and one quadrupole directed towards O5 atom. The electron density of the H1 atom was inspected in the residual electron density map computed with H1 atom omitted. The thermal displacement of the H1 atom was estimated in Fourier residual map to be 1.5 longer in the O-H bond direction vs. the perpendicular ones.

Geometry and charge-density calculations were performed by MoPro;⁶ molecular graphic were prepared using MoProViewer¹¹ and ORTEP-3.¹² Crystallographic and

refinement data are shown in Table S1. Topological bond orders were calculated using the fitted formula¹³

$$n_{\text{topo}} = a + b \lambda_3 + c (\lambda_1 + \lambda_2) + d \rho_{\text{cp}} .$$

Coefficients a , b , c and d were taken from the literature: for C-C bonds $a = -0.522$, $b = -1.695$, $c = 0.00$, $d = 8.473$;¹⁴ for C-O bonds $a = -0.427$, $b = -0.240$, $c = 0.280$, $d = 6.464$;¹⁵ for C-N bonds $a = -0.284$, $b = 0.331$, $c = 0.559$, $d = 6.569$;¹⁴ for N-O bonds $a = -0.628$, $b = 0.505$, $c = 0.448$, $d = 5.275$;¹⁵ for O-H bonds and H \cdots O hydrogen bonds $a = 0.00$, $b = -0.10$, $c = 0.14$, $d = 3.32$.¹⁶

Table S1 Crystallographic, data collection and charge-density refinement details.

Compound	(H ₅ O ₂) ₂ NA·4H ₂ O
Empirical formula	C ₃ H ₇ NO ₇
Formula wt. / g mol ⁻¹	169.085
Crystal dimensions / mm	0.16 x 0.06 x 0.05
Space group	P 2 ₁ /c
$a / \text{\AA}$	3.5787(3)
$b / \text{\AA}$	19.23520(10)
$c / \text{\AA}$	9.1906(8)
$\alpha / ^\circ$	90
$\beta / ^\circ$	93.645(2)
$\gamma / ^\circ$	90
Z	4
$V / \text{\AA}^3$	631.37(8)
$D_{\text{calc}} / \text{g cm}^{-3}$	1.779
μ / mm^{-1}	0.181
Θ range / $^\circ$	2.12 – 45.40
T / K	100(2)
Radiation wavelength	0.71073 (MoK α)

Diffractometer type	Bruker D8 Venture
Range of h, k, l	-7 < h < 6; -36 < k < 38; -16 < l < 12
Reflections collected	66 115
Independent reflections	5323
reflections with $I \geq 2\sigma$	3955
Absorption correction	Analytical
T_{\min}, T_{\max}	0.9750, 0.9920
Weighting scheme	$w = 1/[3.0\sigma^2(F_o^2)]$
R_{int}	0.0727
$R(F)$	0.0309
$R_w(F^2)$	0.0286
Goodness of fit	1.260
H atom treatment	constrained, anisotropic parameters constrained to calculated values
No. of parameters	356
No. of restraints	40
$\Delta\rho_{\max}, \Delta\rho_{\min}$ ($\text{e}\text{\AA}^{-3}$)	0.301; -0.286 rms=0.056

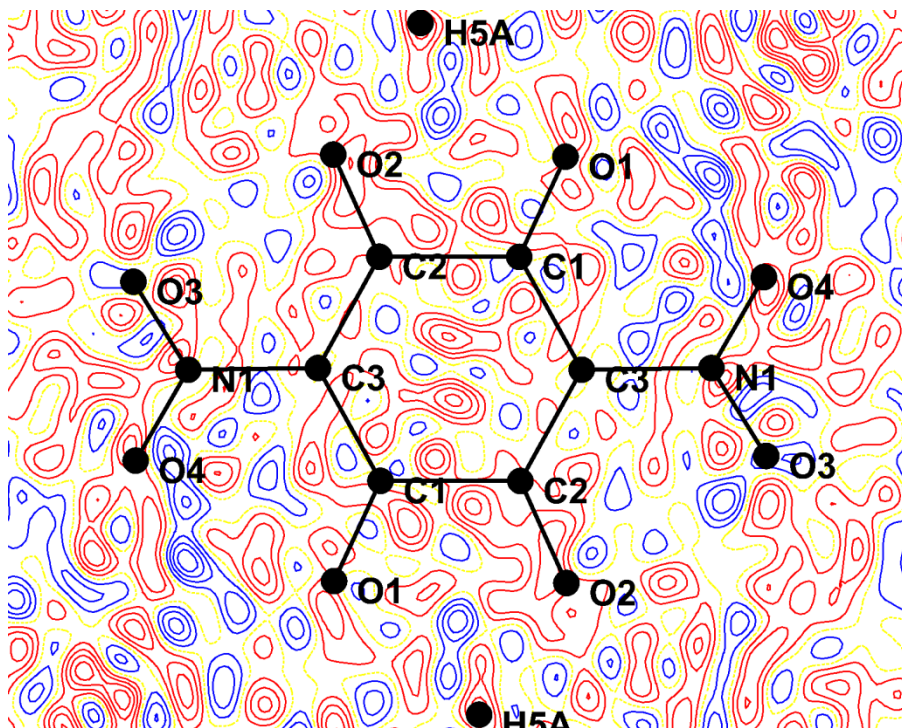


Figure S1 Residual electron density of the nitranilate dianion in the ring plane, with all reflections used. Positive density is shown in blue and negative in red; yellow dotted lines represent zero density. Contours are drawn for $0.05 \text{ e}\text{\AA}^{-1}$.

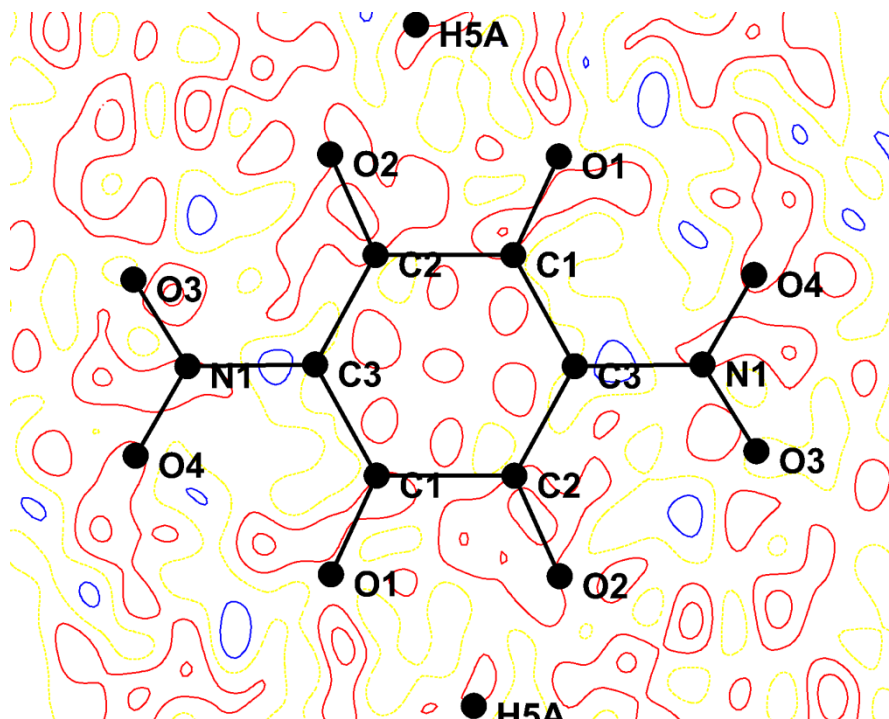


Figure S2 Residual electron density at the nitranilate dianion in the ring plane, with only low-angle reflections ($s < 0.7 \text{ \AA}^{-1}$) used. Positive density is shown in blue and negative in red; yellow dotted lines represent zero density. Contours are drawn for $0.05 \text{ e}\text{\AA}^{-1}$.

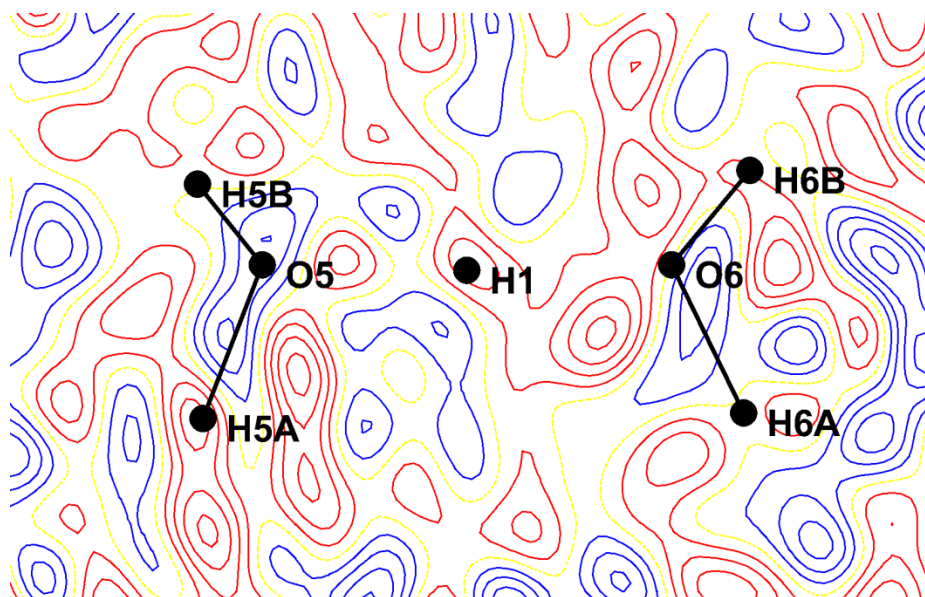


Figure S3 Residual density at the Zundel cation in the plane defined by atoms O5, O6 and H6A, with all reflections used. Positive density is shown in blue and negative in red; yellow dotted lines represent zero density. Contours are drawn for 0.05 eÅ⁻¹.

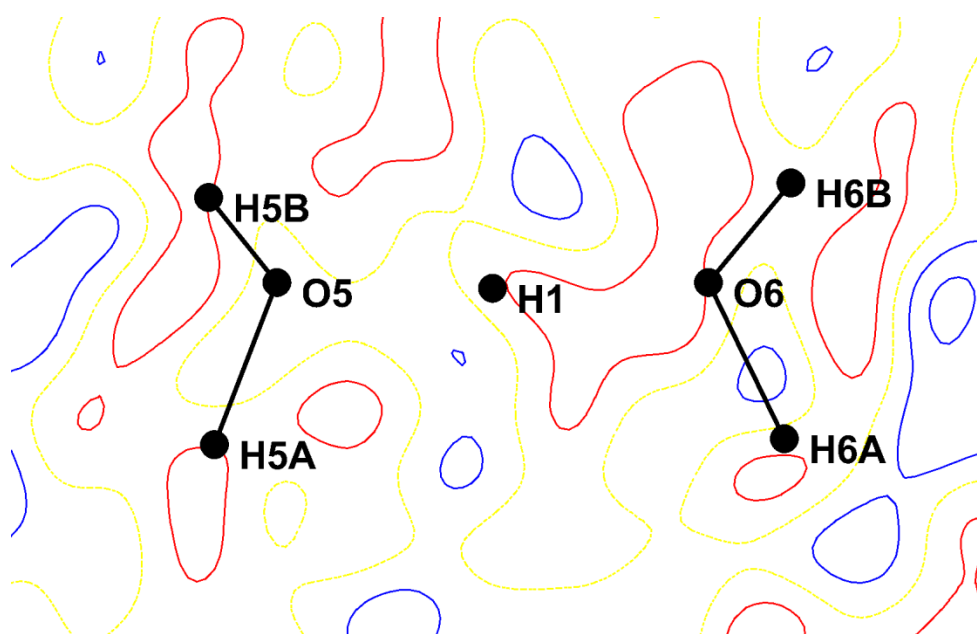


Figure S4 Residual density at the Zundel cation in the plane defined by atoms O5, O6 and H6A, with only low-angle reflections ($s < 0.7 \text{ \AA}^{-1}$) used. Positive density is shown in blue and negative in red; yellow dotted lines represent zero density. Contours are drawn for 0.05 eÅ⁻¹.

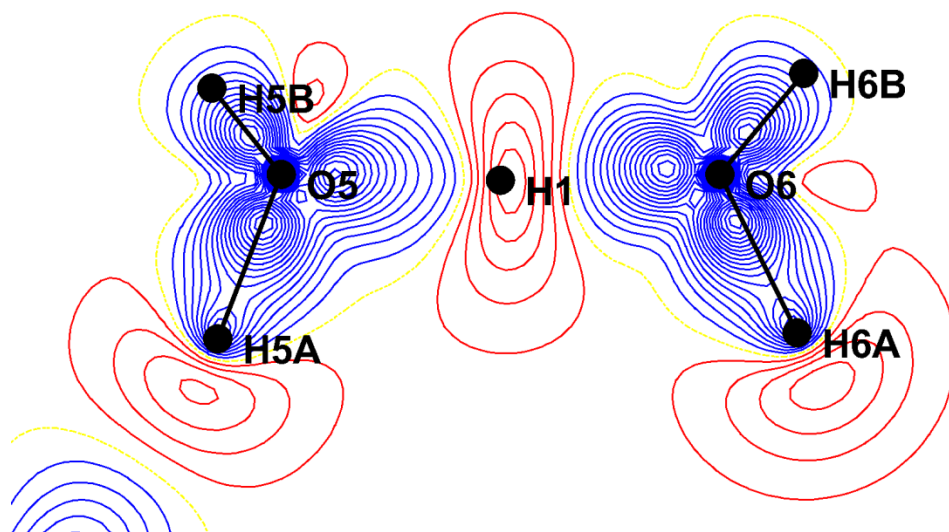


Figure S5 Deformation density of the Zundel cation in the plane defined by atoms O5, O6 and H6A. Positive density is shown in blue and negative in red; yellow dotted lines represent zero density. Contours are drawn for 0.05 eÅ⁻¹.

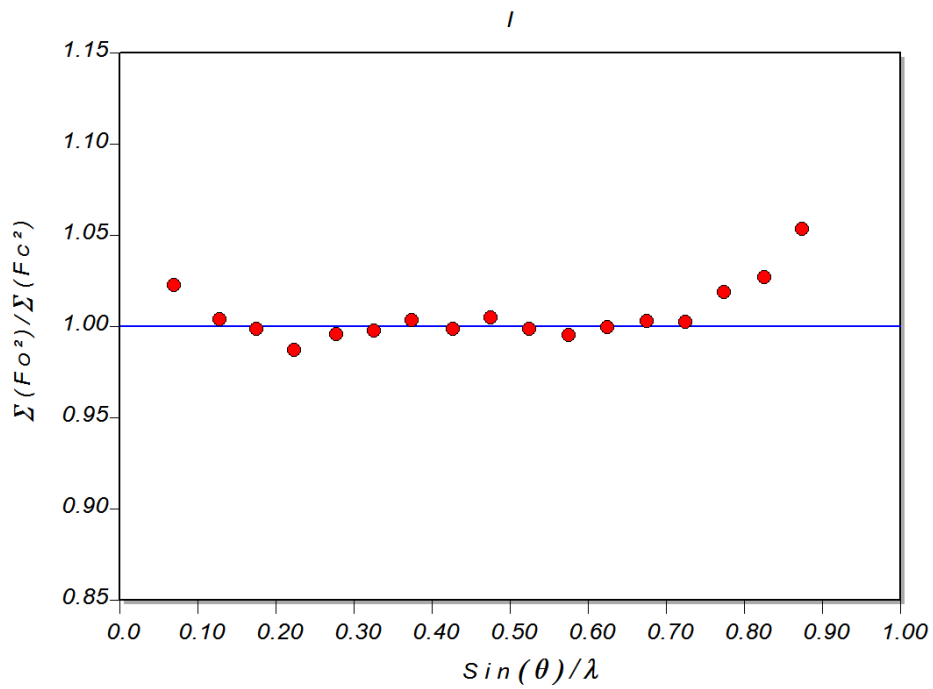


Figure S6 XDRK plot showing the fit of $\langle Y_{\text{obs}} \rangle$ vs $\langle Y_{\text{calc}} \rangle$ as a function of resolution.

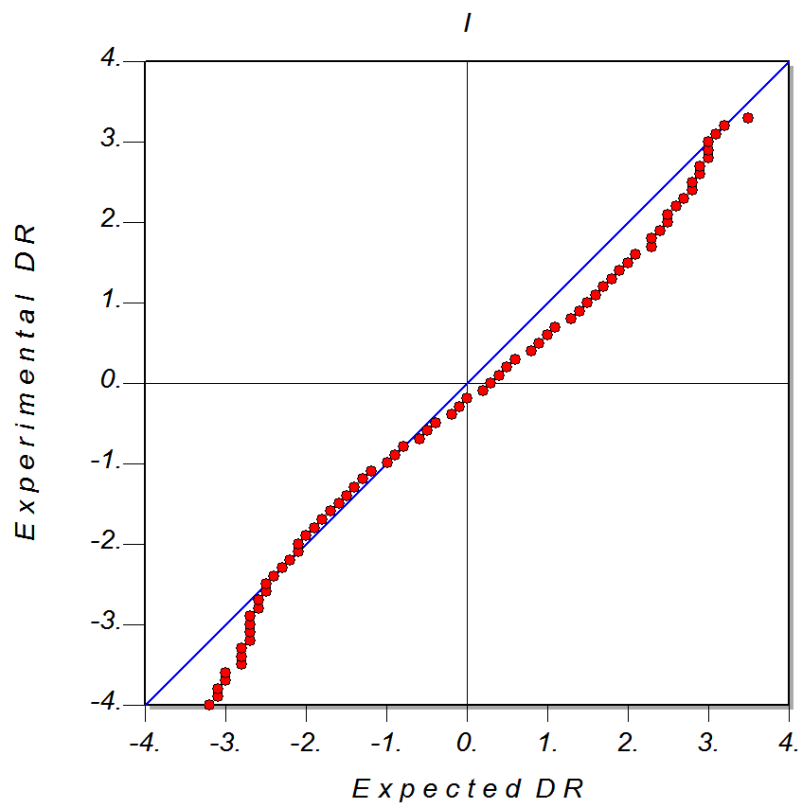


Figure S7 XDRK plot showing the expected and experimental $Y_{\text{obs}} - Y_{\text{calc}}$ data profile. The normal probability plots shows a slight over-representations of reflections with $(Y_{\text{obs}} - Y_{\text{calc}})/\sigma_{Y_{\text{obs}}}$ with large negative values.

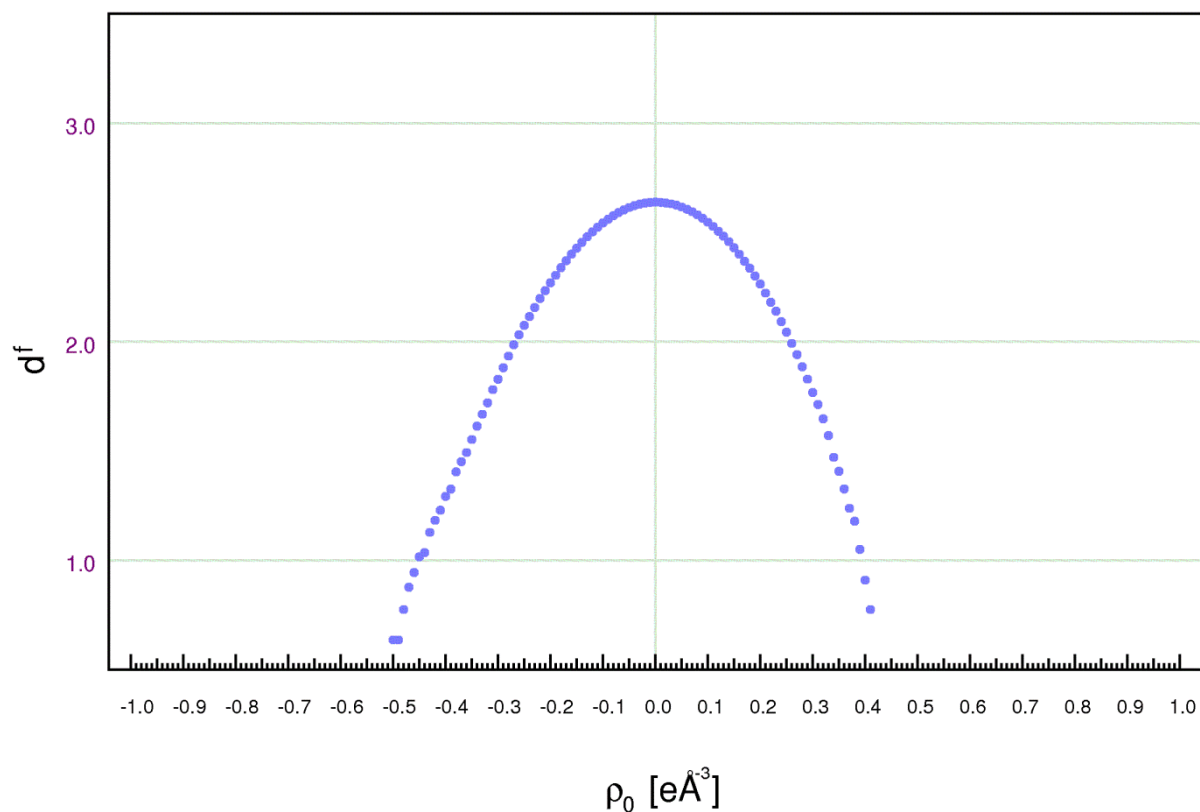


Figure S8 Fractal dimension plot of residual density. The normal probability plots shows a slight over-representations of reflections with $(Y_{\text{obs}} - Y_{\text{calc}})/\sigma_{Y_{\text{obs}}}$ with large negative values.

S2 Periodic DFT calculations

Geometry of the system was optimized in a fixed unit cell using the established plane-wave DFT approach as implemented in the program package VASP 5.3.¹⁷⁻²⁰ The density functional of Perdew, Bruke and Ernzerhof (PBE)²¹ with Grimme's dispersion correction DFT-D3²² was employed together with a plane-wave basis set with kinetic energy cutoff of 500 eV and Projector Augmented Wave atomic pseudopotentials^{23,24}. The integrals in the reciprocal space were computed on a Monkhorst-Pack grid²⁵ consisting of $8 \times 2 \times 4$ k -points. The experimentally determined crystal structure was used as the initial model subject to

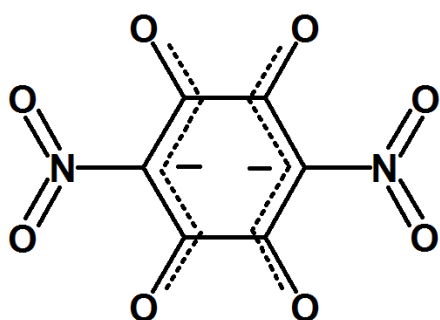
optimization. Both the electron density and electrostatic potential were computed on a grid of $40 \times 216 \times 108$ points and exported to the standard cube format for further analysis. Conversion to the cube format was done by the `chg2cube` script of the VTST Tools package developed by Henkelman Research group of the University of Texas²⁶. The `cif2cell` applet²⁷ was used for the conversion of the experimental structure contained in a CIF file to the geometry input file used by VASP.

To calculate the frequencies and normal modes of vibrations, periodic B3LYP density functional theory (DFT) calculations were performed using the CRYSTAL09 program.²⁸ A preliminary geometry optimization was carried out *via* DFT²⁹ in conjunction with the B3LYP hybrid functional^{30,31} basis set.³² The level of accuracy in evaluating the Coulomb and exchange integrals is controlled by five parameters, for which values of ($ITOL_i = 7, i = 1,4$) and $ITOL_5 = 25$ were used. The shrinking factor of the reciprocal space was set to 8, corresponding to 170 k points in the irreducible Brillouin zone at which the Hamiltonian matrix was diagonalized. Upon energy convergence (10^{-12} Hartree), the periodic wave function based on the optimized geometry was obtained. The coordinates of all atoms were relaxed, but the unit cell parameters were kept fixed. The SHADE3 server was then used to derive U_{ij} tensors of the H atoms in the following way: The normal mode vibrations with frequencies above 200 cm^{-1} were used to calculate the internal mean square displacements of all atoms. The total mean square displacement matrices for the hydrogen atoms were subsequently obtained by combining these internal displacements with external motion, obtained by assuming a riding approximation to the nearest oxygen atom. The standard SHADE procedure, where the internal motion is combined with TLS rigid body motion was not possible for this system, since the TLS analysis requires 5 independent heavy atoms in a rigid (part of a) molecule.

S3 Charge density of the nitranilate dianion

While the Zundel ion is located in a general position, the nitranilate anion (Scheme 1) has a crystallographic symmetry C_i . The electron density of the nitranilate dianion supports the simple model (Scheme 1). Electron-deficient areas of the molecule (Figs. S9 and S10) correspond to single bonds, while electron-rich areas correspond to delocalised systems and nitro-groups. Also, the electrostatic potential (Fig. S10) and atomic charges (Table 1) show that the negative charge is delocalised through the

entire quinoid ring, and also through the nitro groups. The electron-withdrawing effect of the nitro groups is easily noted and is nicely illustrated by topological bond orders (Table S2): the largest concentration of bonding electrons and the greatest bond orders (exceeding 2) belong to N=O bonds. The carbon skeleton is severely electron-depleted, with the formally single bond C1-C2 having a bond order lower than 0.7; formally delocalised bonds C2-C3, C3-C1ⁱ, C1-O2 and C2-O2 have bond orders corresponding to a delocalised π -system, however, significantly lower than 1.5 (which would be expected). This is considerably lower than the corresponding bonds in a similar hydrogen chloranilate anion.³³ Thus, strong acidity of the nitranilic acid (its respective *pKa*'s are -3.0 and -0.5, compared to 0.73 and 3.08 of the chloranilic acid³⁴) which is comparable to sulphuric acid, can be explained by electron-deficiency of its quinoid π -system.



Scheme S1

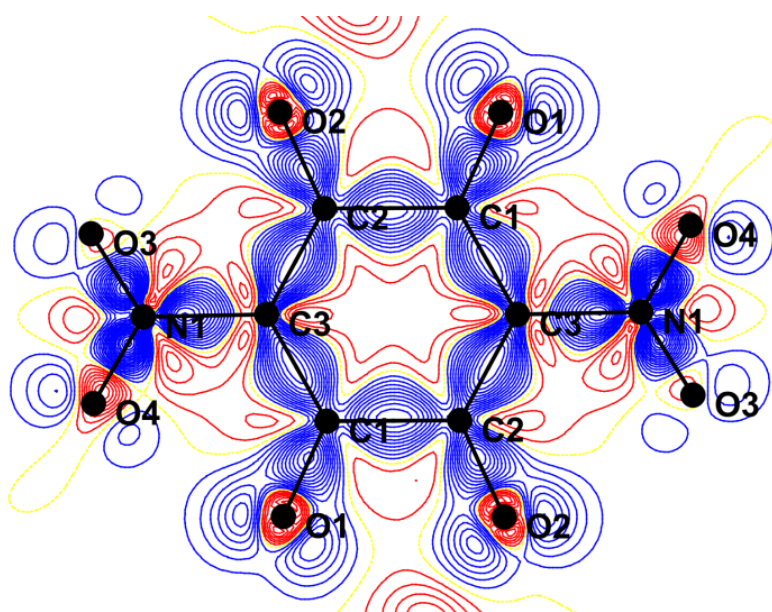


Figure S9 Experimental deformation density of the nitranilate dication in the ring plane. Positive density is shown in blue and negative in red; yellow dotted lines represent zero density. Contours are drawn for $0.05 \text{ e}\text{\AA}^{-1}$. Note that the nitro groups are out of plane.

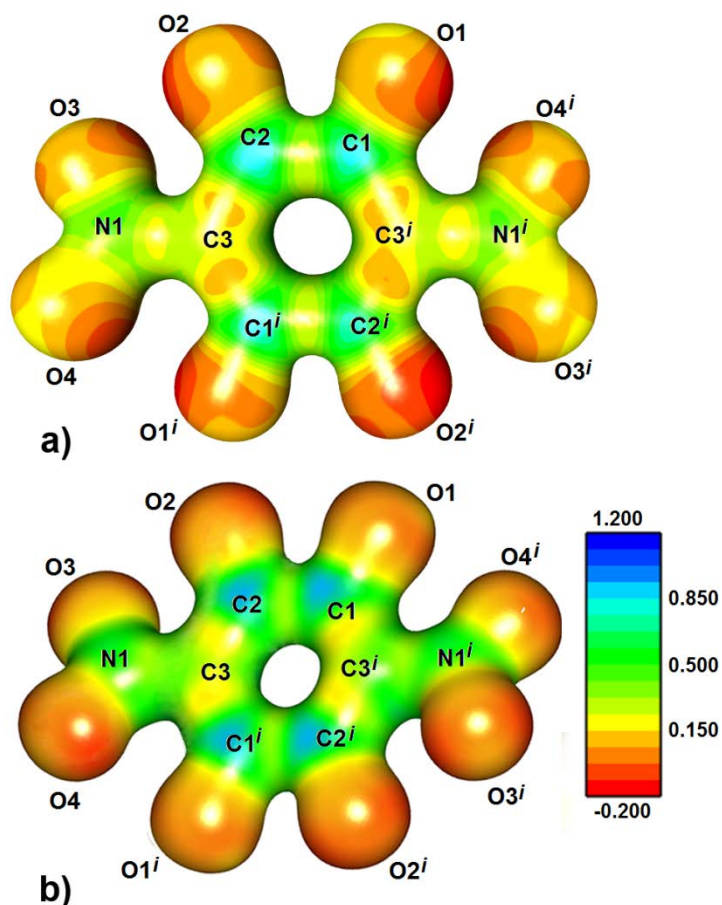


Figure S10 Electrostatic potential generated by a nitranilate dianion mapped on an electron density isosurface of $0.5 \text{ e}\text{\AA}^{-3}$: a) experimental, b) theoretical. Symmetry operators: $i) -x, 1 - y, 1 - z$.

Table S2 Topology of bonds in the nitranilate dianion derived from experimental electron-density after multipole refinement. Symmetry operator: $i) -x, 1-y, 1-z$. Esd's were obtained from the least squares refinement. It has to be recalled here that these esd's are underestimated as shown by Kaminski et al. (2014)³⁵ in a study comparing several structures refined vs. different diffraction data sets collected.

Length (\AA)	Electron Density $\rho(\text{CP}) (\text{e}\text{\AA}^{-3})$	Laplacian $(\text{e}\text{\AA}^{-3})$	Ellipticity	Bond order n_{topo}
-------------------------	---	--	-------------	---------------------------------

C1-C2	1.5539(3)	1.554	-4.9	0.14	0.67
C2-C3	1.4129(2)	2.042	-14.3	0.30	0.90
C3-C1 ⁱ	1.4356(3)	1.918	-11.8	0.32	0.76
C1-O1	1.2293(2)	2.926	-26.8	0.08	1.47
C2-O2	1.2466(2)	2.787	-22.5	0.11	1.38
N1-O3	1.2336(3)	3.367	11.3	0.12	2.31
N1-O4	1.2310(3)	3.2570	9.76	0.10	2.27
C3-N1	1.4414(3)	1.855	-10.9	0.27	1.11

S4 Hirshfeld surface and contacts

The Hirshfeld surface in a crystal is representative of the region in space where molecules come into contact. Therefore, its analysis gives the possibility of obtaining quantitative insights into the chemical nature of intermolecular interactions in the crystalline state. Table S3 shows the percentage of all contact types C_{xy} in the crystal packing and their enrichment E_{xy} .³⁶ An enrichment ratio larger than unity for a given pair of chemical species $X\cdots Y$ indicates that these contacts are over-represented in the crystal packing when compared to equiprobable contacts computed from the chemical composition on the Hirshfeld surface.

The Hirshfeld surface was computed around the different moieties in the crystal and is shown in Fig. S11. Oxygen followed by hydrogen constitute largely the majority of chemical content on the Hirshfeld surface. Consequently hydrogen bonds $H\cdots O$ constitute two thirds of the total interaction surface (Fig. S11).

The four other contact types with surface $> 5\%$ are $O\cdots O$, $H\cdots H$, $C\cdots C$ and $C\cdots O$. All these contacts, except $C\cdots C$, are avoided with E ratios smaller than one ($E < 1$). The $C\cdots C$ hydrophobic contacts are actually over-represented by a factor of six and are related to the significant π -stacking occurring between the organic anions. The $O\cdots O$ contacts are disfavoured at $E = 0.42$ as generally observed³⁶ due to the electrostatic repulsion. In the present crystal structure, they occur mostly between the mildly electronegative O atoms of the nitro groups, while the more negatively charged carbonyl groups do not interact with oxygen. Globally, the crystal structure is

maintained by numerous O··H-O strong hydrogen bonds and by hydrophobic π -stacking.

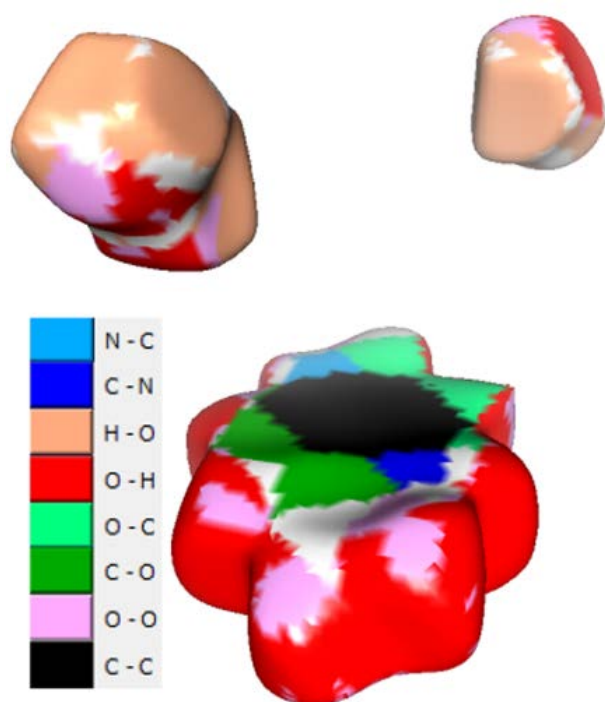


Figure S11 Hirshfeld surfaces around the organic anion, the water molecule and the Zundel cation. The surface is colored according to the major contact types.

Table S3 Statistical analysis of intermolecular contacts. The Hirshfeld surface was computed with the program MoProViewer.⁶ Two HOH, two H_3O^{2+} moieties and one organic anion which are not in contact with each other in the crystal were selected in order to obtain integral surfaces. The second row shows the chemical content on the Hirshfeld surface, followed by C_{xy} , the % of contact types and E_{xy} , their enrichment ratios. The major contacts with $E_{XY} \gg 1$ ratios and correspond to the significantly enriched contacts.

atom	H	C	N	O
% surface	39.6	10.2	2.5	47.7
H	7.0		%	contacts
C	0.5	6.2		

N	0.2	1.4	0	
O	66.6	5.7	3.2	9.2
H	0.42			contacts enrichment
C	0.06	6.2		
N	0.12	2.7	0.00	
O	1.7	0.61	1.4	0.42

S5 References

- 1 K. Molčanov, J. Stare, M. V. Vener, B. Kojić-Prodić, G. Mali, J. Grdadolnik and V. Mohaček-Grošev, *Phys. Chem. Chem. Phys.*, 2014, **16**, 998-1007.
- 2 Bruker, *SAINT*. Bruker AXS Inc., Madison, Wisconsin, USA, 2012.
- 3 Bruker, *SADABS*. Bruker AXS Inc., Madison, Wisconsin, USA, 2001.
- 4 R. H. Blessing, *Crystallogr. Rev.*, 1987, **1**, 3-58.
- 5 G. M. Sheldrick, *Acta Crystallogr. A*, 2008, **64**, 112-122.
- 6 C. Jelsch, B. Guillot, A. Lagoutte and C. Lecomte, *J. Appl. Crystallogr.*, 2005, **38**, 38-54.
- 7 B. Niepötter, R Herbst-Irmer & D. Stalke, *J. Appl. Cryst.*, 2015, **48**, 1485-1497.
- 8 F. Pascale, C. M. Zicovich-Wilson, F. Lopez, B. Civalleri, R. Orlando and R. Dovesi, *J. Comput. Chem.*, 2004, **25**, 888-897.
- 9 C. M. Zicovich-Wilson, F. Pascale, C. Roetti, V.R. Saunders, R. Orlando and R. Dovesi, *J. Comput. Chem.*, 2004, **25**, 1873-1881
- 10 A. Ø. Madsen, H. O. Sørensen, C. Flensburg, R. F. Stewart and S. Larsen, *Acta Cryst. A*, 2004, **A60**, 550-561.
- 11 B. Guillot, *Acta Crystallogr. A*, 2012, **68**, s204; B. Guillot, F. Enrique, K. Huder and C. Jelsch, *Acta Cryst. A*, 2014, **70**, C279.

- 12 L. J. Farrugia, *J. Appl. Crystallogr.*, 1997, **30**, 565.
- 13 B. Zarychta, Z. Zaleski, J. Kyzioł, Z. Dazskiewicz and C. Jelsch, *Acta Cryst. B*, 2011, **B67**, 250-262.
- 14 S. T. Howard and O. Lamarche, *J. Phys. Org. Chem.*, 2003, **16**, 133-141.
- 15 V. G. Tsirelson, E. V. Bartashevich, A. I. Stash and V. A. Potemkin, *Acta Crystallogr. B*, 2007, **B63**, 142-150.
- 16 E. V. Bartashevich, D. K. Nikulov, M. V. Vener and V. G. Tsirelson, *Comp. Theor. Chem.*, 2011, **973**, 33-39.
- 17 G. Kresse and J. Hafner, *J. Phys. Rev. B*, 1993, **47**, 558-561.
- 18 G. Kresse and J. Hafner, *J. Phys. Rev. B*, 1994, **49**, 14251-14269.
- 19 G. Kresse and J. Furthmüller, *Comput. Mat. Sci.*, 1996, **6**, 15-60.
- 20 G. Kresse and J. Furthmüller, *Phys. Rev. B*, 1996, **54**, 11169-11186.
- 21 J. P. Perdew, K. Burke and M. Ernzerhof, *Phys. Rev. Lett.*, 1996, **77**, 3865-3868.
- 22 S. Grimme, *J. Comp. Chem.* 2006, **27**, 1787-1799.
- 23 P. E. Blochl, *Phys. Rev. B*, 1994, **50**, 17953-17979.
- 24 G. Kresse and D. Joubert, *Phys. Rev. B*, 1999, **59**, 1758-1775.
- 25 H. J. Monkhorst and J. D. Pack, *Phys. Rev. B*, 1976, **13**, 5188-5192.
- 26 D. Sheppard, P. Xiao, W. Chemelewski, D. D. Johnson, and G. Henkelman, *J. Chem. Phys.* 2012, **136**, 074103.
- 27 T. Björkman, *Comput. Phys. Commun.*, 2011, **182**, 1183-1186.
- 28 R. Dovesi, R. Orlando, B. Civalleri, C. Roetti, V. R. Saunders and C. M. Zicovich-Wilson, *Z. Kristallogr.*, 2005, **220**, 571-573.
- 29 P. Hohenberg, *Phys. Rev.*, 1964, **136**, B864-B871.
- 30 C. Lee, W. Yang, and R. G. Parr, *Phys Rev B.*, 1988, **37**, 785-789.
- 31 A. D. Becke, *J. Chem. Phys.*, 1993, **98**, 5648.
- 32 P. C. Hariharan, and J. A. Pople, *Theor. Chim. Acta.*, 1973, **28**, 213-222.

- 33 K. Molčanov, J. Stare, B. Kojić-Prodić, C. Lecomte, S. Dahaoui, C. Jelsch, E. Wenger, A. Šantić and B. Zarychta, *CrystEngComm*, 2015, **17**, 8645-8656.
- 34 K. Wallenfels and K. Friedrich, *Chem. Ber.*, 1960, **93**, 3070-3082.
- 35 R. Kamiński, S. Domagała, K. N. Jarzemska, A. A. Hoser, W. F. Sanjuan-Szklarz, M. J. Gutmann, A. Makal, M. Malińska, J. M. Bąk and K. Woźniak. *Acta Cryst.*, 2014, **A70**, 72-91.
- 36 C. Jelsch, K. Ejsmont and L. Huder, *IUCr J.*, 2014, **1**, 119-128.